Supporting Information

Engineering Interfacial Structures to Accelerate Hydrogen Evolution Efficiency of MoS_2 over a Wide pH Range

Shasha Li[a,b], Suchada Sirisomboonchai[c], Xiaowei An[c], Xuli Ma[d], Peng Li[a], Lixia Ling[e], Xiaogang Hao[e*], Abuliti Abudula[c], Guoqing Guan[b,c*]

[a] College of Chemical and Biological Engineering, Taiyuan University of Science and Technology, Taiyuan 030024, China.

[b] Energy Conversion Engineering Laboratory, Institute of Regional Innovation (IRI), Hirosaki University, 2-1-3, Matsubara, Aomori 030-0813, Japan.

[c] Graduate School of Science and Technology, Hirosaki University, 1-Bunkyocho, Hirosaki 036-8560, Japan.

[d] College of Environmental Science and Engineering, Taiyuan University of Technology, Taiyuan, Shanxi 030024, China.

[e] Department of Chemical Engineering, Taiyuan University of Technology, Taiyuan 030024, China.

***Corresponding authors**

E-mails: xghao@tyut.edu.cn (X. Hao); guan@hirosaki-u.ac.jp (G. Guan).

1. Experimental section

1.1 Reagents and chemicals

Cobalt nitrate hexahydrate ($Co(NO_3)_2·6H_2O$, 99%), urea ($CO(NH_2)_2$), ammonium fluoride (NH_4F), thioacetamide (C_2H_5NS, ＞98%), and disodium molybdate (VI) dihydrate ($Na_2MoO_4·2H_2O$) purchased from Wako, Japan were used to fabricate the electrocatalysts without further purification. Sulfuric acid (H_2SO_4, 98%), potassium hydroxide (KOH) (Sigma-Aldrich, Japan), disodium hydrogen phosphate (Na_2HPO_4), and sodium dihydrogen phosphate dihydrate ($NaH_2PO_4·2H_2O$) were respectively dissolved in deionized water and used as the electrolytes for electrochemical characterizations of the electrode. The commercial 20 wt% Pt/C catalyst and Nafion solution (5 wt%) were purchased from Sigma-Aldrich, Japan. All chemicals were used as received. The deionized water (18.2 MΩ cm) was used in all the experiments. Carbon paper (CP) (Toray, Japan) cut as 2 cm × 2 cm dimension was used as the electrode substrate, which was immersed in sulfuric acid for 3 h at first and then in ethanol for another 3 h to improve its hydrophilicity prior to deposition.

1.2. Co(OH)F nanowires coated CP electrode (Co(OH)F/CP)

As shown in Fig. 1, Co(OH)F was firstly grown on the pretreated CP sheet (2 cm × 2 cm) by a hydrothermal synthesis method. In a typical process, 2 mmol of $Co(NO_3)_2·6H_2O$, 10 mmol of $CO(NH_2)_2$ and 8 mmol of NH_4F were dissolved in 36 mL of deionized water under vigorous stirring for 30 min. Then, the solution was transferred into a Teflon-lined stainless autoclave (50 mL) with a piece of CP (2 cm × 2 cm; which was cleaned again by ethanol for 20 min prior to use). The autoclave was sealed and heated at 120 °C for 12 h in an electric oven, and then cooled down to room temperature naturally. Finally, the electrocatalyst coated CP was taken out from the autoclave, and after thoroughly washed with deionized water, it was dried at 70 °C for 6 h. Herein, the obtained Co(OH)F nanowires coated CP was denoted as Co(OH)F/CP.

1.3. Heterostructured CoS_2@MoS_2 catalysts coated CP electrode (CoS_2@MoS_2/CP)

Firstly, 1 mmol of $Na_2MoO_4·2H_2O$ and 4 mmol of C_2H_5NS were dissolved in 30 mL of deionized water with ultrasonic treatment for 10 min until a homogeneous solution was obtained. Then, the solution was transferred into a Teflon-lined stainless autoclave (50 mL) to immerse the above prepared Co(OH)F/CP sheet (cut into two pieces with an area of 1 cm × 1 cm). The autoclave was heated at 200 °C for 24 h. The resulting CoS_2@MoS_2/CP sheet was washed with deionized water thoroughly followed by vacuum drying. The loading amount of CoS_2@MoS_2 on carbon paper substrate was estimated to be ~ 2.4 mg cm^{-2}. Moreover, the layer of MoS_2 growth on the CoS_2 was controlled by optimizing the molar ratio of $Na_2MoO_4{\cdot}2H_2O$ and C_2H_5NS (other two cases were: 1 mmol $Na_2MoO_4{\cdot}2H_2O$ and 2 mmol C_2H_5NS, 1mmol $Na_2MoO_4{\cdot}2H_2O$ and 6 mmol C_2H_5NS). From the SEM image (Fig.S3), in the case of the ratio of Mo:S = 1:2, a thin layer of MoS_2 generated on the surface of CoS_2/CP, the amounts of MoS_2 was too low to form enough interface active sites, resulting in the limited enhancement of HER activity. With the further increase of the ratio of Mo:S = 1:6, the MoS_2 layer became too thick so that the CoS_2@MoS_2 interfaces would be hard to expose, which suppressed the HER activity. Thus, the thickness of MoS_2 layer played a key role in enhancing the catalytic activity for the HER performance.

For comparison, CoS_2/CP was also prepared using the similar procedure without adding $Na_2MoO_4{\cdot}2H_2O$. Meanwhile, MoS_2/CP was prepared where the pretreated CP (1 cm ×1 cm) was used instead of Co(OH)F/CP.

1.4. 20 wt% Pt/C coated CP electrode (20 wt% Pt/C/CP)

20 mg of commercial 20 wt% Pt/C powder was dispersed in the 87 μL of 5 wt% Nafion, 261 μL of ethanol and 652 μL of deionized water, followed with ultrasonic treatment for 60 min until a homogeneous dispersion was achieved. Then, 100 μL of the dispersion was loaded onto the pretreated CP, and dried in air overnight at room temperature. The loading amount of 20 wt% Pt/C catalyst on CP was ~ 2.0 mg cm^{-2}, just the same as that of CoS_2@MoS_2 on CP.

1.5. Physical Characterizations

Morphology and elemental distributions were carried out by a scanning electron microscopy (SEM, Hitachi SU8010) system equipped with a Horiba Scientific energy dispersive spectrometer (EDS). Nanostructures were investigated by a JEM-2100F Transmission electron microscopy (TEM, JEOL, Japan). For the preparation of sample for TEM measurement, the sample was peeled off from CP and dispersed in ethanol at first, and then the solution was dropped onto a copper grid and dried naturally. The crystalline structure was determined by X-ray diffraction (XRD, Rigaku SmartLab X-Ray Diffractometer) using a Cu-K (λ=1.5405 Å) radiation source. The Raman spectrum was recorded using a high-resolution Raman spectrometer (Thermo Fischer DXR). The valence states of the elements were characterized using X-ray photoelectron spectroscopy (XPS) with a VG Scientific ESCALab250i-XL unit (UK).

1.6. Electrochemical performance test

Voltammetric measurement was carried out using a VersaSTAT 4 potentiostat galvanostat electrochemical workstation (Princeton, USA) with a standard three-electrode cell, employing the as-prepared electrode (CP, Co(OH)F/CP, MoS_2/CP, CoS_2/CP, CoS_2@MoS_2/CP or 20 wt% Pt/C/CP) as the working electrode and Pt wire (or graphite rod) as the counter electrode. Ag/AgCl was used as the reference electrode in acid and neutral solutions but Hg/HgO electrode was used as the reference electrode in alkaline solution. All the experiments were carried out at ambient temperature without the activation process. Before the electrochemical test, the real potential of the reference electrode was determined in the electrolyte (Fig. S3). The potentials reported in this study were calibrated to the values based on the reversible hydrogen electrode (RHE) using the conversion formula in 0.5 M H_2SO_4 solution, E(RHE) = E(Ag/AgCl) + 0.226 V, in 1.0 M PBS solution, E(RHE) = E(Ag/AgCl) + 0.197 + 0.64 V, in 1.0 M KOH solution, E(RHE) = E (Hg/HgO) + 0.924 V for Ag/AgCl and Hg/HgO reference electrodes, respectively. Polarization curves were obtained using linear sweep voltammetry (LSV) curves conducted in the acid, alkaline, neutral electrolytes with a scan rate of 2 mV s^{-1} and then corrected by the *iR* loss according to the following equation: $E_{corr} = E_{mea} - iR$. The potentials reported in this work were expressed vs. RHE. Electrochemical impedance spectroscopies (EISs) were measured within a frequency range of 0.01 Hz to 0.1 MHz in the 0.5 M H_2SO_4, 1.0 M KOH and 1.0 M PBS aqueous solutions, respectively. Unless specifically mentioned, the voltammograms were recorded with the *iR* drop compensation. Chronoamperometric curves were recorded at a constant current density without the *iR* drop compensation. The electrochemical active surface areas (ECSAs) were determined from the capacitance measurements in the potential region of no faradic process at different scan rates of 5, 10, 15, 20, 25 and 30 mV/s, respectively.

The number of active sites and turnover frequency (TOF, s^{-1}) of catalysts were calculated by an electrochemical approach through cyclic voltammetry measurements in pH = 7 phosphate buffer at a scan rate of 50 $mV \cdot s^{-1}$, according to the previous reported method [1].

$$n = \frac{Q}{F} \cdot \frac{1}{2} \cdot \frac{1}{m} = \frac{i \cdot t}{F} \cdot \frac{1}{2} \cdot \frac{1}{m} = \frac{i \cdot \frac{V}{u}}{F} \cdot \frac{1}{2} \cdot \frac{1}{m} = \frac{10 \cdot S}{F \cdot m}$$

(1)

The per-site turnover frequency (s^{-1}) was calculated by the following equation:

$$N = \frac{Q}{F} \cdot \frac{1}{2} = \frac{i \cdot t}{F} \cdot \frac{1}{2} = \frac{i \cdot \frac{V}{u}}{F} \cdot \frac{1}{2} = \frac{10 \cdot S}{F}$$

(2)

$$TOF = \frac{j}{F \cdot N} \cdot \frac{1}{2} \qquad (3)$$

Herein, n is the number of active sites ($mol \cdot g^{-1}$ catalyst); *Q* the integrated charge from cyclic voltammogram in pH = 7 phosphate buffer; F the Faraday constant (96485 $C \cdot mol^{-1}$); and *i, V, t, u, S, m, j,* and *N* are the current (A), potential (V), sweep time (s), sweep rate ($V \cdot s^{-1}$), integrated effective area in cyclic voltammogram recorded in pH = 7 phosphate buffer after deduction of the blank value for CP, the mass of active component in the catalyst, the current (A) during the linear sweep measurement in 0.5 M H_2SO_4, and the total number of active sites (mol), respectively.

Faraday efficiency (FE) was determined by a drainage gas collecting method. The quantity of H_2 gas production was measured by the electrolyzer, where the gas evolution rate was measured by a soap-film gas flowmeter and converted to mole by ideal gas law. For comparison, the theoretical amount of hydrogen gas generated was calculated by Faraday`s law assuming that all charges that passed through the working electrode were $2e^-$. Then FE was calculated by the following equation:

$$FE = \frac{2nF}{Q} \qquad (4)$$

where, n is the amount of hydrogen generated (mol); Q the total amount of charge passed through the cell (C); and F Faraday constant (96485 $C \cdot mol^{-1}$).

1.7. Density functional theory (DFT) Calculations

The computations for density functional theory (DFT) calculations were performed using the *Vienna Ab initio Simulation Package* (VASP) code with the RPBE exchange correlation functional and projector-augmented plane wave (PAW) pseudopotentials. The RPBE function was chosen in order to obtain reasonable adsorption energies. The Brillouin zone was sampled using a 2 × 2 × 1 Monkhorst-Pack grid for the geometry optimizations and a 7 × 7 × 1 Monkhorst-Pack grid for the calculations of electronic properties. A plane-wave basis set with the cut-off energy of 400 eV was chosen. The convergence criteria for energies and forces were set to 1.0×10^{-6} eV and −0.01 eV/Å, respectively. Spin-polarization was considered for all the simulations.

The free energy of hydrogen adsorption (ΔG_{H*}) was calculated as follows [2]:

$$\Delta G_{H*} = \Delta E_{H*} + \Delta E_{ZPE} - T\Delta S$$

where ΔE_{H*} is the hydrogen binding energy. ΔE_{ZPE} is the difference in zero point energy between the adsorbed and the gas phase, which can be obtained from vibrational frequency calculation as implemented in VASP. $T\Delta S$ was estimated to be 0.24 eV to consider the entropy change at room temperature. Hence, the formula was simplified as follows:

$$\Delta G_{H*} = \Delta E_{H*} + 0.24$$

Different to the acid solution, the first step of HER in the alkaline solution is water dissociation to facilitate the generation of adsorbed H^*. The climbing-image nudged elastic band (CI-NEB) method was used to search for transition states and determine the energy barrier of water dissociation step.

The key reaction steps in the alkaline HER through Volmer-Heyrovsky mechanism:

Volmer step: $H_2O + e^- + {}^*$ ✂ $H^* + OH^-$

Heyrovsky step: $H_2O + e^- + H^*$ ✂ ${}^* + H_2 + OH^-$

Here, * denotes a site on the slab models. The free energy for Step (1) and (2) should be the same at equilibrium potential of HER. Under this assumption, one can avoid computation of the exact free energy of OH^- in solutions by using computational hydrogen electrode [3].

Herein, four main stage are considered: initial state, activated water adsorption, H^* intermediates formation, H_2 formation [4]. The free energies (at the reduction potentials U_0=0 V vs RHE) were calculated as follows:

$G_0 = G(^*) + G(H_2O)$

$G_1 = G(H\text{-}OH^*)$

$G_2 = G(H^*) + G(OH^-)$

$G_3 = G(^*) + G(OH^-) + 1/2\,G(H_2)$

and $G_0 = G_3$.

Herein, the ΔG_{H2O} ($\Delta G_{H2O}=G_1-G_0$) value is applied as an activity descriptor for the Volmer step. Tthe species H-OH is a ground state of activated water adsorption. The ΔG_{H*} ($\Delta G_{H*}= G_2-G_3$) value was utilized as an activity descriptor for the Tafel step or Heyrovsky step [5].

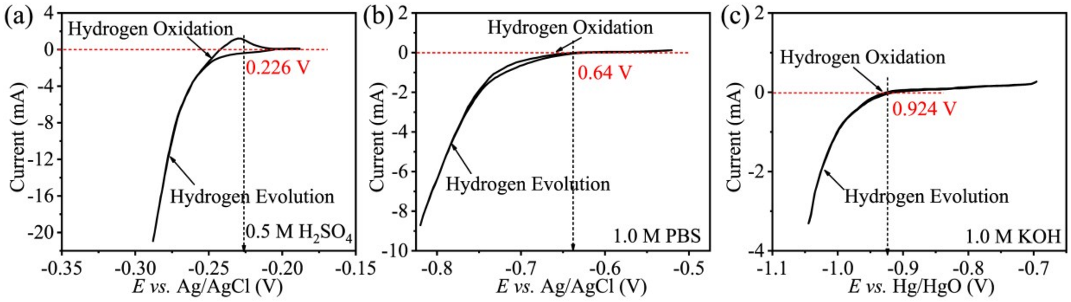

Fig. S1. Reference electrode calibrations. Reference electrode calibrations in (a) 0.5 M H_2SO_4 solution, E (RHE) = E (vs. Ag/AgCl) + 0.226 V, (b) 1.0 M PBS solution, E(RHE) = E (vs. Ag/AgCl) + 0.64 V, (c) 1.0 M KOH solution, E (vs. RHE) = E (vs. Hg/HgO) + 0.924 V.

Calibration of SCE and conversion to RHE. The calibration of SCE reference electrode was performed in a standard three-electrode system with the polished Pt wires as the working and counter electrodes, and the SCE as the reference electrode.

Electrolytes were pre-purged and saturated with high purity H_2. CVs were run at a scan rate of 1.0 mV s^{-1}, and the average of the two potentials at which the current crossed zero was taken to be the thermodynamic potential for the hydrogen electrode reactions.

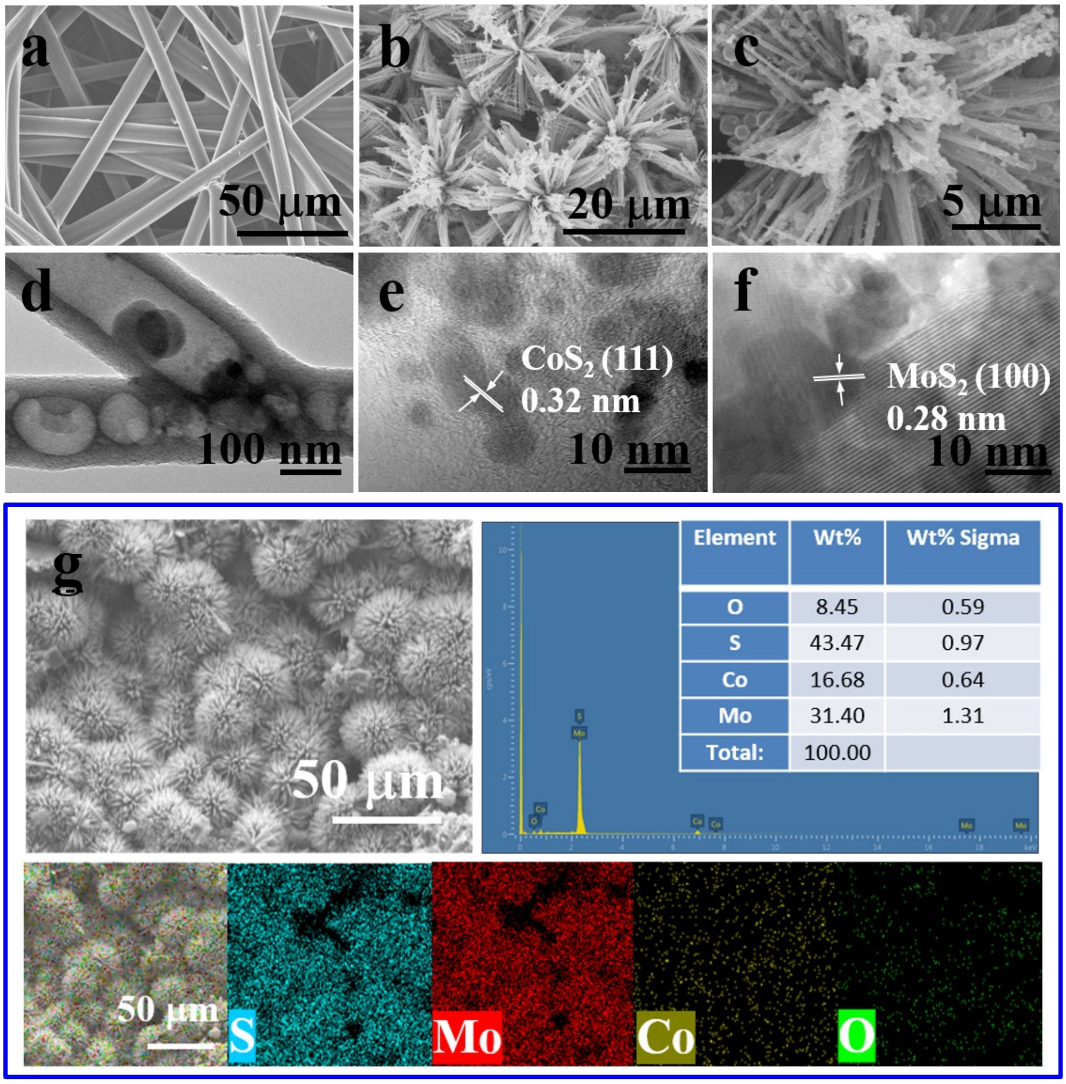

Element	Wt%	Wt% Sigma
O	8.45	0.59
S	43.47	0.97
Co	16.68	0.64
Mo	31.40	1.31
Total:	100.00	

Fig. S2. SEM images of bare CP (a) and CoS_2/CP (b-c). TEM images of Co(OH)F (d), CoS_2 (e) and MoS_2 (f). (g) Element distribution mappings of Co, Mo, S and O in the sample of CoS_2@MoS_2/CP.

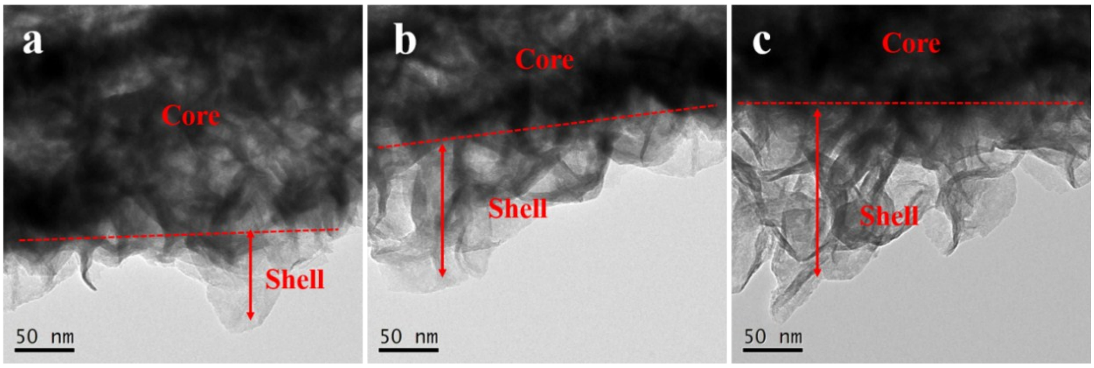

Fig. S3. High-magnification TEM images of $CoS_2@MoS_2$ nanocomposites by optimizing the ratio of Mo and S for the deposition of MoS_2 layer at different ratios : (a)1:2, (b)1:4, (c)1:6.

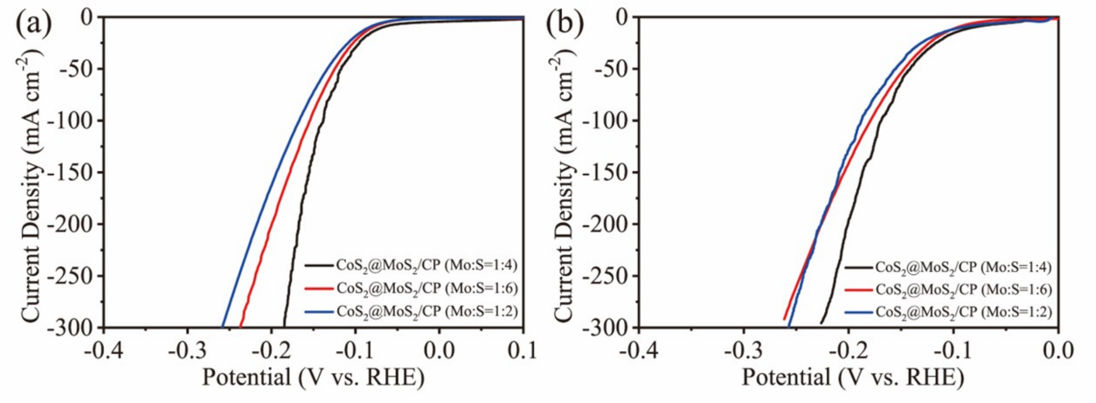

Fig. S4. Polarization curves of $CoS_2@MoS_2$/CP electrode measured by optimizing the ratio between Mo and S for the deposition of MoS_2 layer at different ratios in (a) 0.5 M H_2SO_4 and (b) 1.0 M KOH electrolytes.

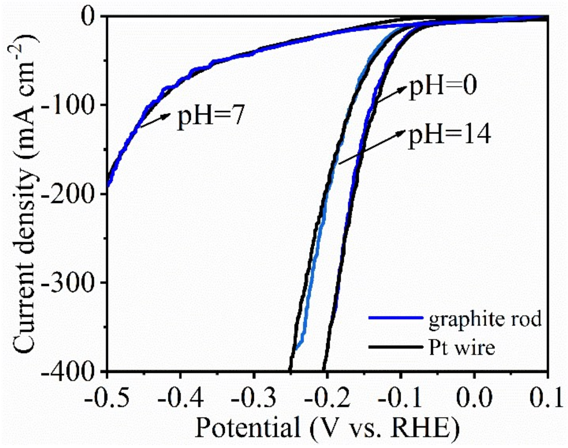

Fig. S5. Polarization curves of $CoS_2@MoS_2/CP$ electrode measured in a wide pH range solution using Pt wire and carbon rod as the counter electrode respectively.

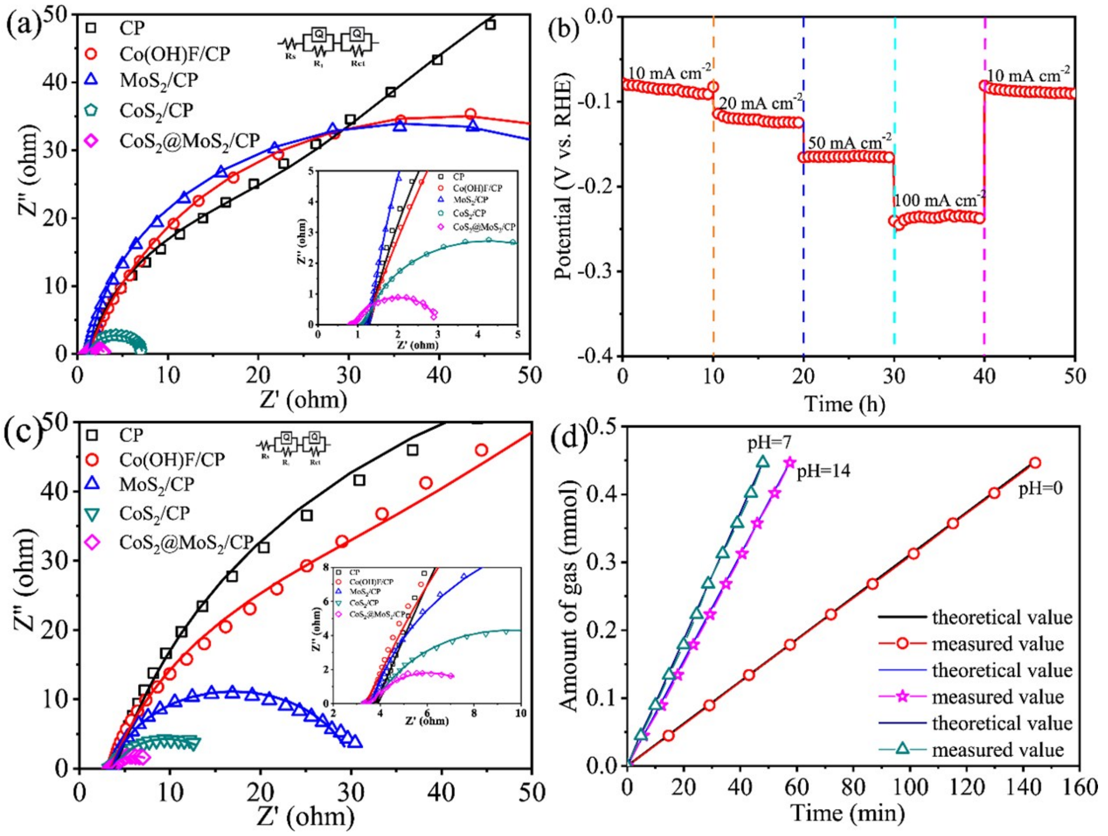

Fig. S6. (a) Nyquist plots (overpotential = 200 mV) for the samples in alkaline electrolyte. (b) The electrochemical stability of the $CoS_2@MoS_2/CP$ catalyst measured by chronopotentiometry at different current densities in 1.0 M KOH. (c) Nyquist plots (overpotential = 200 mV) for the samples in 1.0 M PBS (pH = 7). (d) Amounts of H_2 theoretically calculated and experimentally measured versus time for $CoS_2@MoS_2/CP$ under the current density of 10 mA cm^{-2} in 0.5 M H_2SO_4 (j = 10 mA cm^{-2}), 1.0 M KOH (j = 25 mA cm^{-2}) and 1.0 M PBS (j = 30 mA cm^{-2}), respectively.

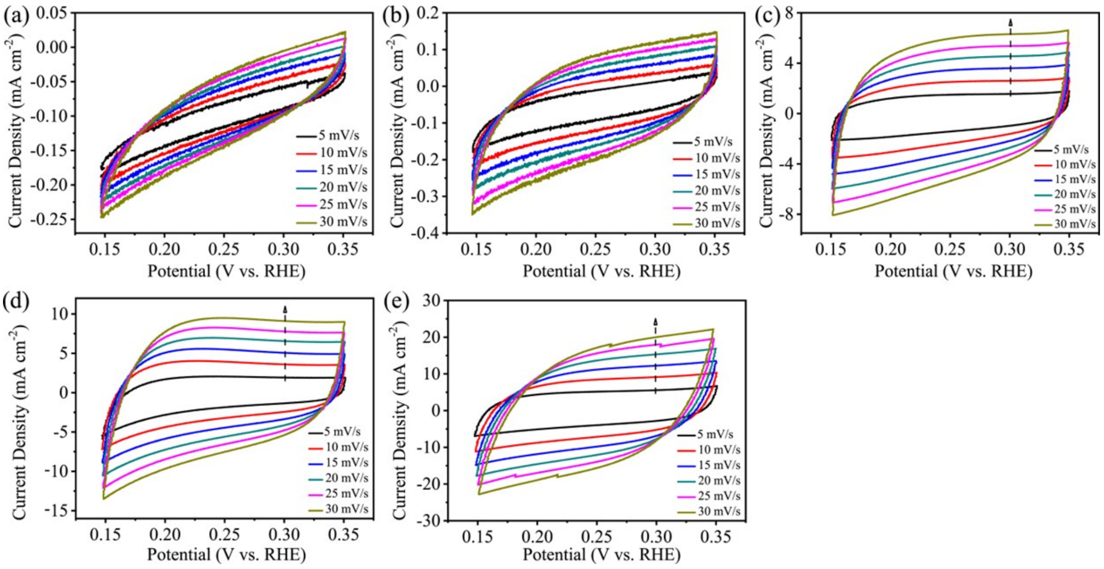

Fig. S7. CVs of bare CP (a), Co(OH)F/CP (b), MoS_2/CP (c), CoS_2/CP (d) and CoS_2@MoS_2/CP (e) composite electrodes between the potential regions of 0.15 and 0.35 V (vs Ag/AgCl) with scan rates of 5, 10, 15, 20, 25, and 30 mV s^{-1} in 0.5 M H_2SO_4 solution.

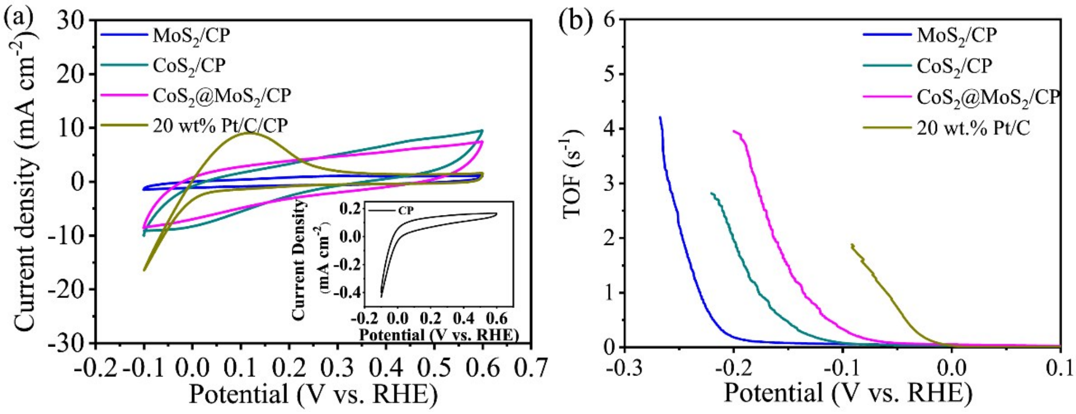

Fig. S8. (a) CVs of MoS_2/CP, CoS_2/CP, CoS_2@MoS_2/CP and 20 wt% Pt/C/CP and bare CP (inset) in 1.0 M PBS (pH = 7) with a scan rate of 50 mV s^{-1}. (b) Turn over frequency (TOF) curves of the MoS_2/CP, CoS_2/CP, CoS_2@MoS_2/CP and 20 wt% Pt/C/CP.

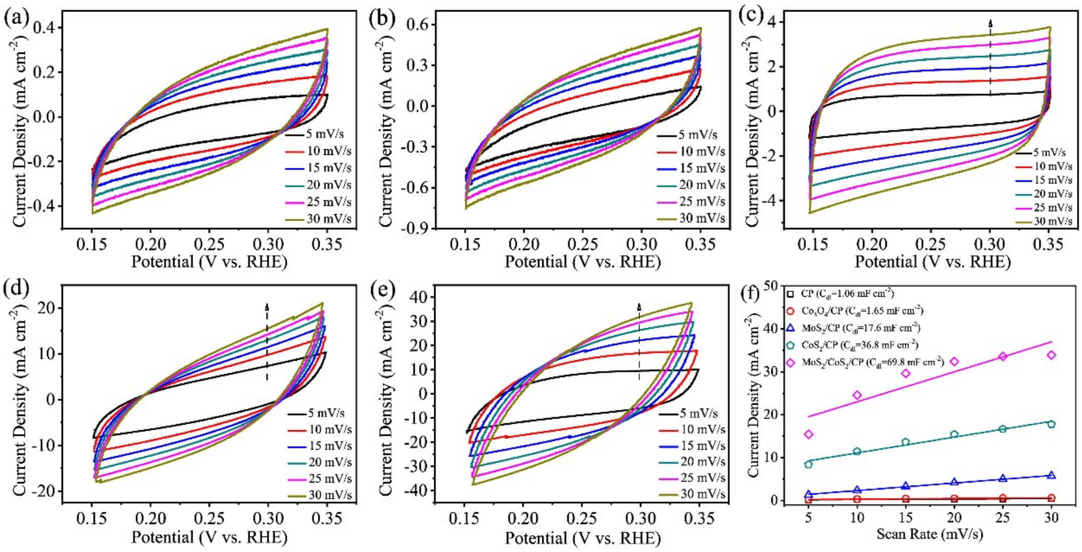

Fig. S9. CVs of bare CP (a), Co(OH)F/CP (b), MoS_2/CP (c), CoS_2/CP (d) and CoS_2@MoS_2/CP (e) composite electrodes between the potential regions of 0.15 and 0.35 V (vs Hg/HgO) with scan rates of 5, 10, 15, 20, 25, and 30 mV s^{-1} in 1.0 M KOH solution.

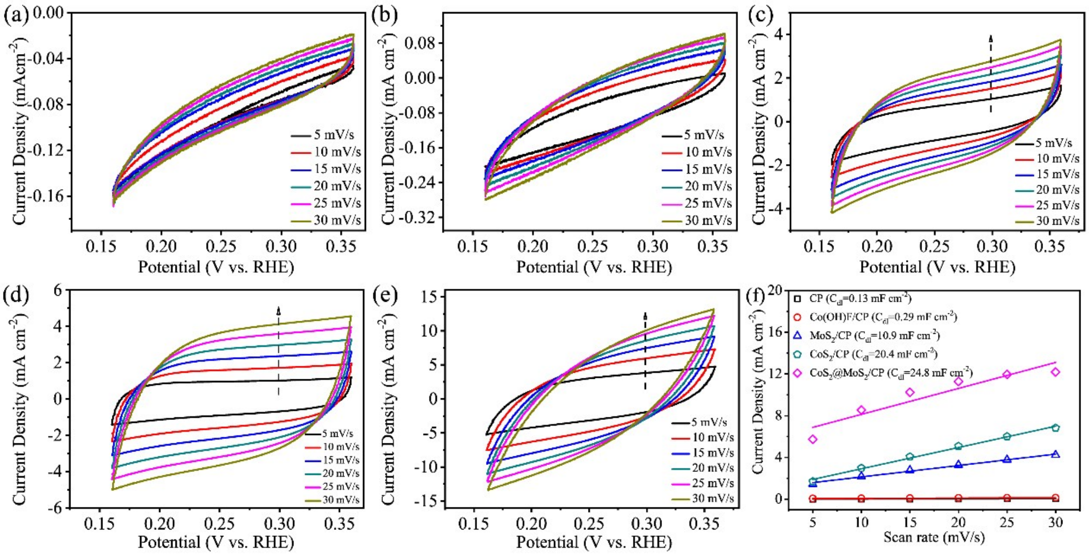

Fig. S10. CVs of bare CP (a), Co(OH)F/CP (b), MoS_2/CP (c), CoS_2/CP (d) and CoS_2@MoS_2/CP (e) composite electrodes between the potential regions of 0.15 and 0.35 V (vs Ag/AgCl) with scan rates of 5, 10, 15, 20, 25, and 30 mV s^{-1} in 1.0 M PBS solution.

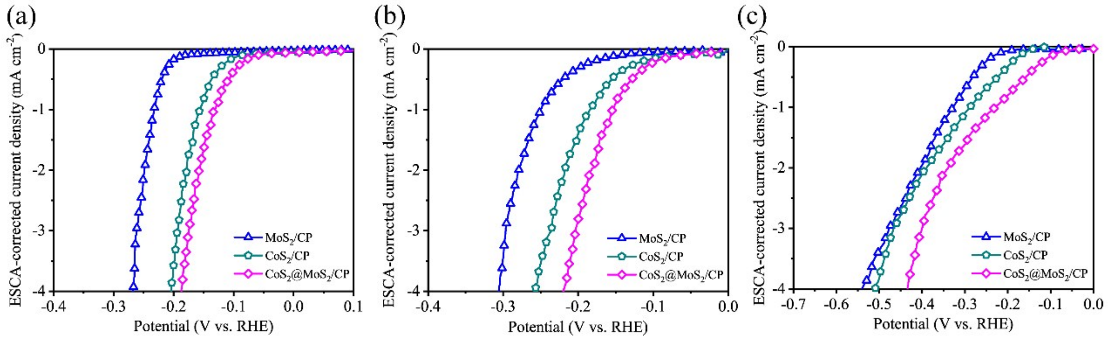

Fig. S11. LSV curves normalized by ECSA of MoS$_2$/CP, CoS$_2$/CP and CoS$_2$@MoS$_2$/CP in 0.5 M H_2SO_4 (a), 1.0 M KOH (b) and 1.0 M PBS solution (c), respectively.

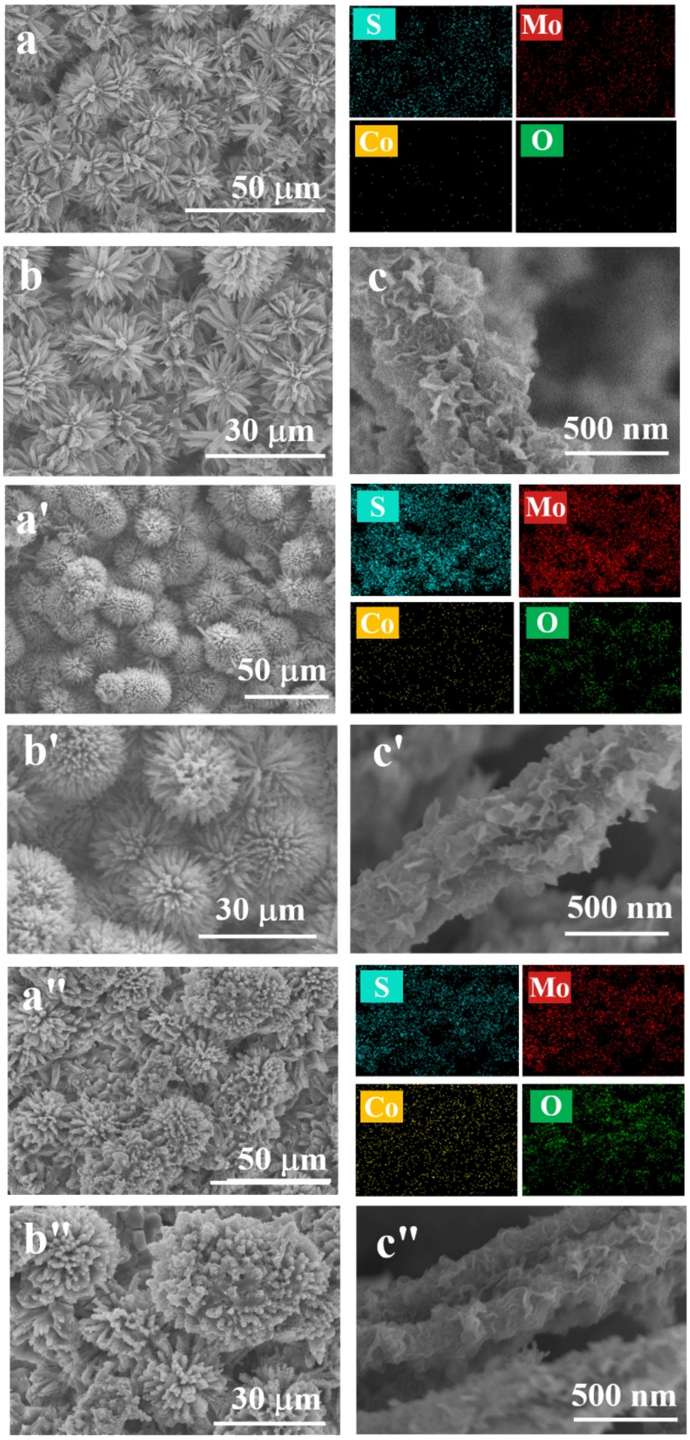

Fig. S12. Characterizations after the stability test. SEM images of CoS_2@MoS_2/CP after the long-term 48 h stability test at the current density of 10 mA cm^{-2} in the 0.5 M H_2SO_4 solution (a-c), 1.0 M PBS solution (a′-c′) and 1.0 M KOH solution (a′′-c′′), and the corresponding EDS elemental mappings of the electrode, respectively.

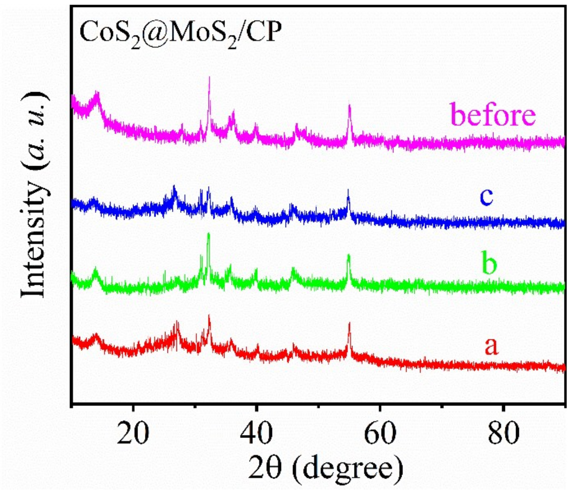

Fig. S13. Characterizations after the stability test. X-ray diffraction (XRD) patterns of CoS_2@MoS_2/CP after the HER stability test under the current density of 10 mA cm^{-2} in (a) 0.5 M H_2SO_4, (b) 1.0 M PBS and (c) 1.0 M KOH solution, respectively.

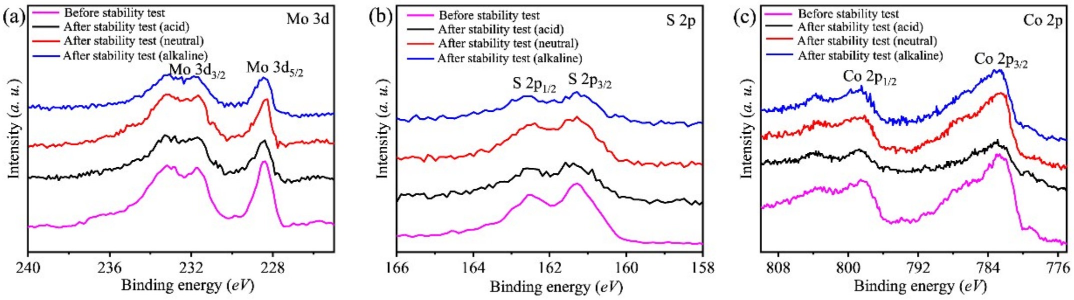

Fig. S14. Characterizations after the stability test. High-resolution XPS spectra of (a) Mo 3d, (b)S 2p and (c) Co 2p for CoS_2@MoS_2/CP after the HER stability test under the current density of 10 mA cm^{-2} in 0.5 M H_2SO_4, 1.0 M PBS and 1.0 M KOH solution, respectively.

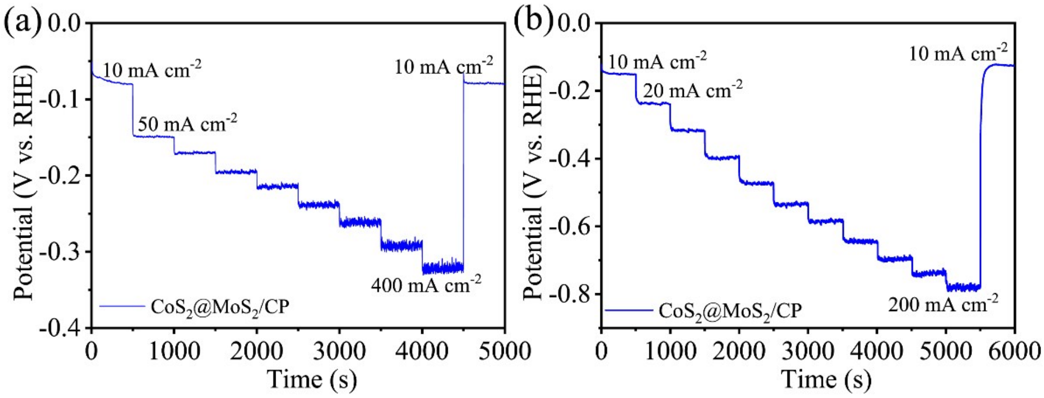

Fig. S15. HER multi-step chronopotentiometric curves of CoS$_2$@MoS$_2$/CP without *iR* compensation). The current density starts at 10 mA cm^{-2} and ends at 400 mA cm^{-2} with an increment of 50 mA cm^{-2} every 500 s in 1.0 M KOH electrolyte (a). The current density starts at 10 mA cm^{-2} and ends at 200 mA cm^{-2} with an increment of 20 mA cm^{-2} every 500 s in PBS electrolyte (pH =7) (b).

Table S1. The $\Delta E(H^*)$, ΔZPE, $T\Delta S$ and $\Delta G(H^*)$ values of the H^* at the S adsorption sites on the (001) surface of CoS_2 (200), MoS_2 (002), CoS_2@MoS_2 and Pt (111).

Surface	Adsorption site	$\Delta E(H^*)$/eV	ΔZPE/eV	$T\Delta S$	$\Delta G(H^*)$/eV
CoS_2	S	-2.0219961	0.10893	0.196231	-1.7168351
MoS_2	S	1.6814139	0.0639225	0.1957205	1.9410569
CoS_2@MoS_2	Interface S	0.1256739	0.0913095	0.1968205	0.4138039
CoS_2@MoS_2	Non-interface S	-1.1752261	0.0913095	0.1968205	-0.8870961
Pt	Pt	-0.3310361	0.0028105	0.1962075	-0.1320181

Table S2. Comparison of the overpotential at η = 10 mA cm^{-2} with other recently reported non-noble mental electrocatalysts with high HER performance HER in 0.5 M H_2SO_4, 1.0 M PBS, and 1.0 M KOH aqueous solutions.

Catalyst	**Overpotential (mV)/ η=10mA cm^{-2}**			**Reference**
	0.5M H_2SO_4 (PH=0)	**1.0M PBS (PH=7)**	**1.0M (KOH) PH=14**	
CoS_2@MoS_2/CP	69	145	82	This work
MoP_2 NPs/Mo	273	211	194	[6]
MoN@NPCNCs	72	84.85	80.18	[7]
MnMoO4 NSA/NF	89	161	105	[8]
Mo-Ni_2P nanowire/NF	67	84	78	[9]
V-CoP/CC	47	123	71	[10]
Mo_2C@NC	124	156	60	[11]
Co-NRCNTs	260	540	370	[12]
Mn-Co-P/Ti	49	86	76	[13]
$Zn_{0.30}Co_{2.70}S_4$	80	85	90	[14]
WP NAs/CC	130	200	150	[15]
CoP/CC	67	106	209	[16]
CoP/NiCoP/NC	60	123	75	[17]
$FePSe_3$/NC	70	140.1	118.5	[18]
$(Fe_xNi_{1-x})_2P$/NF	81	90	103	[19]
Co-Fe-P	86	138	66	[20]
MoP/NPG	148	150	126	[21]

References

[1] X. Dai, K. Du, Z. Li, M. Liu, Y. Ma, H. Sun, X. Zhang, Y. Yang, *ACS Appl. Mater. Interfaces*, 2015, **7**, 27242-27253.

[2] J.K. Nørskov, T. Bligaard, A. Logadottir, J. Kitchin, J.G. Chen, S. Pandelov, U. Stimming, *J. Electrochem. Soc.*, 2005, **152**, J23-J26.

[3] Y. Zheng, Y. Jiao, Y. Zhu, L.H. Li, Y. Han, Y. Chen, M. Jaroniec, S.Z. Qiao, *J. Am. Chem. Soc.*, 2016, **138**, 16174-16181.

[4] J. Zhang, T. Wang, P. Liu, S. Liu, R. Dong, X. Zhuang, M. Chen, X. Feng, *Energy Environment. Sci.*, 2016, **9**, 2789-2793.

[5] B. Zhang, J. Liu, J. Wang, Y. Ruan, X. Ji, K. Xu, C. Chen, H. Wan, L. Miao, J. Jiang, *Nano Energy*, 2017, **37**, 74-80.

[6] Z. Pu, I. Saana Amiinu, M. Wang, Y. Yang, S. Mu, *Nanoscale*, 2016, **8**, 8500-8504.

[7] M.-Q. Wang, C. Tang, C. Ye, J. Duan, C. Li, Y. Chen, S.-J. Bao, M. Xu, *J. Mater. Chem. A*, 2018, **6**, 14734-14741.

[8] L. Wen, Y. Sun, T. Zhang, Y. Bai, X. Li, X. Lyu, W. Cai, Y. Li, *Nanotechnology*, 2018, **29**, 335403.

[9] Y. Sun, L. Hang, Q. Shen, T. Zhang, H. Li, X. Zhang, X. Lyu, Y. Li, *Nanoscale*, 2017, **9**, 16674-16679.

[10] X. Xiao, L. Tao, M. Li, X. Lv, D. Huang, X. Jiang, H. Pan, M. Wang, Y. Shen, *Chem. Sci.*, 2018, **9**, 1970-1975.

[11] Y. Liu, G. Yu, G.D. Li, Y. Sun, T. Asefa, W. Chen, X. Zou, *Angew. Chem. Int. Ed. Engl.*, 2015, **54**, 10752-10757.

[12] X. Zou, X. Huang, A. Goswami, R. Silva, B.R. Sathe, E. Mikmekova, T. Asefa, *Angew. Chem. Int. Ed. Engl.*, 2014, **53**, 4372-4376.

[13] T. Liu, X. Ma, D. Liu, S. Hao, G. Du, Y. Ma, A.M. Asiri, X. Sun, L. Chen, *ACS Catal.*, 2016, **7**, 98-102.

[14] Z.-F. Huang, J. Song, K. Li, M. Tahir, Y.-T. Wang, L. Pan, L. Wang, X. Zhang, J.-J. Zou, *J. Am. Chem. Soc.*, 2016, **138**, 1359-1365.

[15] Z. Pu, Q. Liu, A.M. Asiri, X. Sun, *ACS Appl. Mater. Interfaces*, 2014, **6**, 21874-

21879.

[16] J. Tian, Q. Liu, A.M. Asiri, X. Sun, *J. Am. Chem. Soc.*, 2014, **136**, 7587-7590.

[17] R. Boppella, J. Tan, W. Yang, J. Moon, *Adv. Funct. Mater.*, 2018, **29**, 1807976.

[18] J. Yu, W.-J. Li, H. Zhang, F. Zhou, R. Li, C.-Y. Xu, L. Zhou, H. Zhong, J. Wang, *Nano Energy*, 2019, **57**, 222-229.

[19] W. Zhang, Y. Zou, H. Liu, S. Chen, X. Wang, H. Zhang, X. She, D. Yang, *Nano Energy*, 2019, **56**, 813-822.

[20] J. Chen, J. Liu, J.-Q. Xie, H. Ye, X.-Z. Fu, R. Sun, C.-P. Wong, *Nano Energy*, 2019, **56**, 225-233.

[21] R. Ge, J. Huo, T. Liao, Y. Liu, M. Zhu, Y. Li, J. Zhang, W. Li, *Appl. Catal. B: Environ.*, 2020, **260**, 118196.